Detection of 3D-inhomogeneities of the medium at magnetotelluric sounding in the Arctic (numerical experiment)

Valery V. Plotkin, Vladimir S. Mogilatov, Vladimir A. Gurev and Vladimir V. Potapov

A.A. Trofimuk Institute of Petroleum Geology and Geophysics, Siberian Branch of Russian Academy of Sciences, Koptug ave. 3, Novosibirsk, 630090, Russia. E-mail: PlotkinVV@ipgg.sbras.ru

SUMMARY

The magnetotelluric sounding (MTS) conducted on drifting ice floes in the Arctic is of particular interest for detection of 3D-inhomogeneities in crustal conductivity. Their manifestations in behavior of standard magnetotelluric curves are shielded by the well conducting layers of seawater and sediment. As target objects, these inhomogeneities are shown as small changes (only one-hundredths of percent) in apparent resistivity, and as very weak variations of vertical magnetic field component. Therefore, accounting for additional data on the vertical electric field component or the electric field potential of the transverse magnetic (TM) mode is of interest. For recording the TM-mode potential, we offer to use the circular electric dipole (CED) located on the ice surface as a receiver in MTS. We investigate possibilities of crustal 3D-inhomogeneity detection using the TM-mode potential received with the CED. A numerical experiment showed that the potential of electric field of the TM-mode on the ice surface reaches values suitable for detection. Examples of the inverse problem solution using synthetic data on the TM-mode field are presented. We found that the information on the depth of 3D-object could be obtained by the analytical continuation of the profile data on the TM-mode potential. Using the MTU-5 Phoenix Geophysics stations for the CED system, we carried out preliminary measurements on the ice surface on the Ob river. We checked the measurement results of the TM-mode potential using the MTS data obtained earlier near the CED system. We compared results of the TM-mode potential calculation for the found 3D-medium model to the CED experimental data. Our results showed that the potential dependences on the period measured by the CED and those obtained for the 3D-model have similar characteristics. We believe recording the TM-mode potential in the Arctic allows to reveal the existence and characteristics of crustal conductivity 3D-heterogeneities.

Key words*:* Magnetotellurics; Arctic region; Inverse theory

Issue Section: Marine geosciences and applied geophysics

INTRODUCTION

Magnetotelluric soundings (MTS) have been carried out in Arctic regions since this method introduction, primarily in onshore survey points (for example, Hoffman & Horton 1966; Trofimov & Fonarev 1976; Evans et al. 2005; Beka et al. 2015). Nevertheless, the structure of the Arctic ocean floor in the context of searches for minerals has been of great interest. This also requires performing measurements from the sea ice surface and thereby testing this technology under extreme conditions.

Simultaneous observations of the horizontal components of the magnetic field and of two components of telluric current were made on Arctic drifting station Charlie during the winter of 1959-1960 and on station Arlis I in early 1961 (Swift & Hessler 1964). The sea ice surface represents a large, stable, nonmagnetic and relatively nonconducting platform for performing magnetic and telluric current measurements. The Charlie telluric current electrodes consisted of two perpendicular pairs spaced about 1000 meters. On Arlis I, the electrodes were spaced 200 meters. The inference was made that the presence of electric currents in deeper water at a distance of some hundred kilometers away seems to affect the experimental data.

The magnetotelluric experiment was carried out on the Lomonosov Ridge (Fütterer 1992), with the instrumentation deployed on a large ice floe and the electrodes placed a few meters below the ice. Performing magnetotelluric measurements in the Arctic was challenging in many ways: (1) the proximity of the sources might invalidate the requirement for a uniform source field; (2) attenuation of electromagnetic radiation in seawater restrains the resolution at depth; (3) sea ice drift, entailing movements of the magnetometers in the static magnetic field which can induce noise in the data.

The Arctic magnetotelluric experiment was carried out with an aim to obtain information on the conductivity of the crust and mantle beneath the Gakkel Ridge rift valley (Thiede 2002). The major problem in this experiment was that the strength of the natural long-period source signal, which is produced in the Earth ionosphere, is significantly attenuated by the high conductivity of seawater. This effect decreases with increasing wavelength. Therefore, long observation times are necessary to achieve good results. Since the duration of MTS experiments needs to be long enough, the problems of fitting in with the vessel's schedule were unavoidable.

For the sub-sea permafrost studies in the Arctic shelf, attenuation of high-frequency variations in the water layer is an essential limiting factor for MTS application at a large sea depth (Piskunova et al. 2018).

Carrying out the MTS surveys in Antarctica was challenging due to a very high contact impedance of ice in the electric field measurement. The difficult acquisition of electric field data on ice was overcome using a custom made electrometer system, with preamplifiers located at the electrode sites (Wannamaker et al. 1996). Non-plane-wave effects in the data were suppressed using a robust jackknife procedure that emphasized outlier removal from the vertical magnetic field records (Wannamaker et al. 2004). The magnetic fields were measured using high-moment induction coils similar to land operation records (Wannamaker et al. 2017).

Magnetotellurics (MT) with its wide bandwidth is ideally suited for addressing problems occurring over broad depth scales in Polar Regions but collecting MT data at high latitudes presents challenges unique to these regions (Hill 2018). In addition, Hill (2018) notes the generation of 'blizstatic', localised random electric fields caused by the spin drift of moving charged snow and ice particles which produce significant noise in the electric fields during periods of strong winds.

The MTS applications to the heterogeneous Arctic ocean floor were examined with the use of 3D quantitative modeling (Korotaev et al. 2010). This allowed an inference that the MTS is effective for research works in the Arctic ocean for determination of the type of the Earth crust underlying the water layer. However, the MTS measurements from the sea ice cover cannot find 3D-inhomogeneities in the crust because of the low resolution of MTS curves.

Variations of five components of the electromagnetic field are usually recorded during MTS. The MTS method is based on the Tikhonov-Cagniard model for a horizontally-layered medium excited by a vertically propagating plane wave. This primary field belongs to the transverse electric (TE) mode, in which the vertical electric field component is equal to zero. With the standard approach, transfer functions are defined as ratios between horizontal components of electric $E_{x,y}$ and magnetic fields $H_{x,y}$. Deviations from the Tikhonov-Cagniard basic model are defined by the fifth recorded component – the vertical component of magnetic field H_z.

Vertically propagating primary wave induces current flow in the 3D-medium. It is observed in the transverse magnetic (TM) mode, in which the vertical electric field component is presented. The electrical

conductivity of the atmosphere is very low σ_a ~ 10^{-14} S/m. Currents are equal to zero in the nonconductive atmosphere. Therefore, the TM-mode horizontal electric field components recorded on the land surface are associated only with deviations from the horizontally layered medium. Properties of the different modes to inhomogeneity parameters of the medium can differ in sensitivity considerably (for example, Mogilatov et al. 2016). Thus taking into account additional TM-mode data, in particular, on the TM-mode electric field potential is of interest. For this purpose, in the work (Plotkin & Mogilatov 2019) it is suggested to use the circular electric dipole (CED) located on the land surface.

Application of the CED with its placement on the drifting ice floe in the Arctic is of particular interest (similar to observations carried out earlier at the North Pole stations). The thickness of drifting sea ice in the Arctic is only a few meters, which is much less than Antarctic sea ice thickness. Measurements of the electric field on the drifting ice floe can be carried out using electrodes in seawater. For this purpose, holes for the electrodes were drilled through the ice floe, in order to get a good coupling to the seawater (Thiede 2002). We carried out preliminary measurements on the ice surface on the Ob river using electrodes placed below the ice.

The presence of well conducting seawater and sediment layers shields the underlying 3D-inhomogeneity in standard magnetotelluric surveys. As target objects, such inhomogeneities transpire as slightly changing apparent resistivity, only by one-hundredths of percent. Also, the vertical magnetic field component variations on the sea ice surface are very small: ~ 10^{-3} nT (with a 1 nT amplitude of the primary source wave, Plotkin & Mogilatov 2020). Therefore, the detection of these bodies using a standard approach is almost impossible.

At this, results of these calculations have shown that the TM-mode amplitude potential reaches several μV on the ice surface at shallow sea depths (1 km). It should be noted that the magnetic field of primary source (vertically propagating wave or the average field) on the ice surface in these calculations was (for the sake of concreteness) set to 1 nT. But as the registered potential of TM-mode depends on amplitude and polarization of the primary wave exciting the medium, these estimates will increase in a real situation proportional to amplitudes of components of the primary source horizontal magnetic field. As shown in the work (Plotkin & Mogilatov 2020), it is possible to register values of the TM-mode potential of such order using the CED system with radial lines in the first kilometers. Of course, this requires the magnetic field components recording on the ice surface.

This paper analyzes the possibilities of crustal 3D-inhomogeneity detection taking into account additional data on the TM-mode potential obtained with the CED deployed on the ice floe drifting in the Arctic Ocean.

DETERMINATION OF POTENTIAL OF ELECTRIC FIELD OF TM-MODE

In the work (Plotkin & Mogilatov 2019), the effects taking into account TM-mode were studied using analytical model. From this work, we will use here analytical formulas obtained for TM-mode.

Because of the weak conductivity of the atmospheric air, excitation of the medium by TM-mode is excluded. Therefore, the latter is obviously internal by origin and is connected only with 3D-inhomogeneities of the medium. Let there be, in a uniform half-space with conductivity σ at depth z', a thin conducting layer with total longitudinal conductance $\Sigma(x,y)$ (the OZ axis is directed deep into medium, the ice surface of z=0). The medium conductivity is $\sigma + \sigma'(x,y,z) = \sigma + \Sigma(x,y)\delta(z-z')$, where $\delta(z)$ is the delta function. At $\sigma \gg \sigma'(x,y,z)$ we will apply the perturbation method. The Fourier transformation of the equations allows us to present the electric field as the sum of two modes with Fourier harmonic amplitudes ~$\exp(i\omega t + ik_x x + ik_y y)$ as in (Plotkin et al. 2011):

$$e_x = ik_x e^{TM} + ik_y e^{TE}, \quad e_y = ik_y e^{TM} - ik_x e^{TE},$$

$$e^{TM} = -\frac{ik_x e_x + ik_y e_y}{k_x^2 + k_y^2}, \quad e^{TE} = -\frac{ik_y e_x - ik_x e_y}{k_x^2 + k_y^2}, \tag{1}$$

$$e_z = \frac{k_x^2 + k_y^2}{k^2}\frac{de^{TM}}{dz}, \qquad h_z = -\frac{k_x^2 + k_y^2}{i\omega\mu_0} e^{TE},$$

where designations of amplitudes are introduced: e^{TM} and e^{TE} are potentials of perturbations of electric fields of TM- and TE-mode respectively, $e_{x,y,z}$ and h_z are components of electric and magnetic fields, $k_{x,y}$ are components of a wave vector and $k^2 = k_x^2 + k_y^2 + i\omega\mu_0\sigma$. Apparently, the modes differentiated by the presence of vertical component: electric field in TM-mode and magnetic in TE-mode. With the use

of introduced designations (1), field characteristics boundary registered on the ice surface, are described by the following integrals:

$$U^{TM}(x,y) = \iint dk_x dk_y e^{ik_x x + ik_y y} e^{TM}(k_x, k_y, 0),$$

$$U_z(x,y) = -\iint dk_x dk_y e^{ik_x x + ik_y y} \int_0^\infty e_z\left(k_x, k_y, z\right) dz, \quad (2)$$

$$H_z(x,y) = \iint dk_x dk_y e^{ik_x x + ik_y y} h_z(k_x, k_y, 0),$$

which give distributions at z=0: $U^{TM}(x,y)$ is a TM-mode electric field potential, $H_z(x,y)$ is a TE-mode vertical magnetic field component and $U_z(x,y)$ is a potential registered by means of the virtual infinite vertical line sunk in medium. To calculate integrals (2), we have to receive solutions of the Maxwell equations for the first approach. For this purpose, we used boundary conditions on the ice surface, on infinity and transition boundary conditions (through the thin layer). Substituting the found solutions in (1) and (2), we will obtain the following expressions:

$$U^{TM}(x,y) = -\iint dk_x dk_y e^{ik_x x + ik_y y} \frac{ik_x f_x + ik_y f_y}{(k_x^2 + k_y^2)(k + k_a)} \frac{k_a}{k} e^{-kz\prime},$$

$$U_z(x,y) = -\iint dk_x dk_y e^{ik_x x + ik_y y} \frac{ik_x f_x + ik_y f_y}{k^2(k + k_a)} \frac{k_a}{k} e^{-kz\prime},$$

$$H_z(x,y) = -\frac{1}{i\omega\mu_0} \iint dk_x dk_y e^{ik_x x + ik_y y} \frac{ik_y f_x - ik_x f_y}{k + k_a} e^{-kz'}, \quad (3)$$

$$f_x = E_x^{(0)}(z')\left(i\omega\mu_0 + \frac{k_x^2}{\sigma}\right)\Sigma_k + E_y^{(0)}(z')\frac{k_x k_y}{\sigma}\Sigma_k,$$

$$f_y = E_x^{(0)}(z')\frac{k_x k_y}{\sigma}\Sigma_k + E_y^{(0)}(z')\left(i\omega\mu_0 + \frac{k_y^2}{\sigma}\right)\Sigma_k,$$

where $E_{x,y}^{(0)}(z')$ zero-approaching electric field components of primary vertically propagating plane wave, $k_a^2 = k_x^2 + k_y^2 + i\omega\mu_0\sigma_a$, Σ_k is the Fourier harmonic amplitude of perturbation distribution $\Sigma(x, y)$ and σ_a is an atmosphere conductivity. The given expressions (3) show that potentials U^{TM} and U_z completely coincide on condition of $k_x^2 + k_y^2 \gg i\omega\mu_0\sigma$. This condition is well satisfied at lower frequencies (the long periods) when the skin layer thickness in the uniform half-space is much more, than the characteristic scale of lateral inhomogeneity. As measurements of potentials U^{TM} and U_z are equivalent in such situation, there is no need to drill the well in the medium for registration of vertical electric field component. The suggestion using the CED system on the land surface for measurements of the vertical electric field component is also connected with this circumstance stated in (Plotkin & Mogilatov 2019). Above we meant potential U^{TM} registered by the ideal CED consisting of a continuum of radial lines of the infinite length (Fig. 1). In practice the number of radial lines and their lengths are limited: for application of the CED as a source (Goldman et al. 2015), 8 lines which are uniformly distributed on an azimuth is sufficient. The CED radius is an important characteristic in practice defining the potentials U^{TM} and U_z ratio. Effects of this factor on the CED application as a receiver in MTS were investigated by means of numerical calculations provided in (Plotkin & Mogilatov 2020). It is established that the discussed potential U^{TM} values can be detected using the CED system with radial lines in first kilometers.

DETERMINATION OF PARAMETERS AND LOCATION OF 3D-INHOMOGENEITIES

Let's consider possibilities of the inverse problem solution taking into account the potential U^{TM} data. As 3D-object presence does not affect the behavior of the MTS standard curves, it is possible to determine, using these curves, a normal geoelectric section. Importantly, in the Arctic there is no static shift of the MTS curves, in the absence of near-surface lateral heterogeneities in seawater. The lack of static effect simplifies the identification of the conductive structure in the deep section. We carry out numerical calculations with the model structure used by Plotkin & Mogilatov (2020) and presented in Fig. 2. The

model considers existence of sediment, resistive crust, crustal object and underlying mantle. The sea depth and 3D-heterogeneity were varied in a series of calculations.

We calculate the electromagnetic field in the 3-D non-uniform medium using the Trefftz method (Plotkin & Gubin 2015) and the perturbation method (Plotkin 2017). During the Trefftz method each layer is represented by identical parallelepipeds in which the conductivity is uniform. Their heights are equal to layer thickness. Horizontal sections of the parallelepipeds and their quantity along each horizontal axes (the polygon sizes) control the results accuracy. The choice of polygon sizes is dictated by the characteristics of the studied objects. For example the sizes of polygon shown in Fig. 2 are 110x110 km. There are 11 parallelepipeds along each horizontal axes; the axes are directed to the north (*OX),* to the east (*OY*) and vertically down (*OZ).* For concreteness, the used parallelepiped centers' projections to the ice surface are shown in Fig. 2b by points. It is clear, that time of calculation and necessary memory depends on the number of parallelepipeds. Calculation results of the Trefftz method for the resistivity model are presented in Fig. 3. It shows these value distribution maps on the ice surface and their dependences on the period in points with their maximum perturbations in the presence of 3D-object in the crust. Results are calculated for the magnetic field of the primary wave with 1nT amplitude and polarization along the *OY* axis. Perturbations of the vertical component of the magnetic field and apparent resistivity are negligible, so it is almost impossible to discriminate them. At the same time, the potential of electric field of the TM-mode reaches values suitable for detection. Using such data obtained in several points allows attempting to solve the inverse problem and to determine the properties of the 3D-object.

Analysis of possibilities of the inverse problem solution was carried out using synthetic data on the TM-mode potential by numerical modeling for a predetermined background conductivity structure (Fig. 2) with different 3D-objects in the crust. It was assumed that synthetic experimental data are available for dependences of potential U^{TM} on the period, similar to those shown in Fig. 3, in several points at primary wave independent polarizations along *OX* and *OY* axes.

Given that for the inverse problem solution electromagnetic field calculations are repeated many times, the calculation time was reduced using the perturbation method (Plotkin 2017). Conditions of its applicability are satisfied in case of small deviations of 3D-inhomogeneities from the background medium. Advantages of the perturbation method are connected with the possibility of significant increase in the number of considered spatial harmonics for the field and 3D-heterogeneity representation, and

calculation time reduction. Therefore, to realize more complicated model structure of 3D-heterogeneities shown in Fig. 2 synthetic data are computed using the perturbation method with the increased quantity of reference points up to 111 along *OX* and *OY* axes. The layout scheme of such object is shown in Fig. 4a. Thus, Fig. 4b shows the map of TM-mode potential distribution on the ice surface for the period of 139 s and the primary wave magnetic field polarization along *OY* axis. The sites involved are specified by points with numbers. For two sites, potential dependences on the period are given in Figs 4e and 4f. These dependences are used as synthetic experimental data (specified lines refer to polarizations of the primary wave magnetic field along the *OY* and *OX* axes). In all the cases, the primary wave magnetic field amplitude is 1 nT. Parameters of the object are d_n=2.8 km, h_n=0.2 km.

Of course, for complete recovery of the heterogeneity plan, the data from closely located points are critical, which is not always possible. Therefore, an attempt was made to determine whether it is possible to restore the crustal 3D-object parameters at the inverse problem solution on the larger grid, in particular with the quantity of reference points reduced up to 11 along each horizontal axis.

The optimization of object characteristics was carried out by minimizing the residual functional Φ of potential dependences on the period in the selected sites at both polarizations of primary wave magnetic field:

$$\Phi = \frac{1}{2KJ}\sum_{k=1}^{K}\sum_{j=1}^{J}\left(\left|\frac{lgU^{TM} - lgU_0^{TM}}{lgU_0^{TM}}\right|_{H_{ox}}^2 + \left|\frac{lgU^{TM} - lgU_0^{TM}}{lgU_0^{TM}}\right|_{H_{oy}}^2\right)_{k,j},$$

where U^{TM} and U_0^{TM} are the simulated and experimental TM-mode potentials, respectively, obtained at different stations (summation over *k*) and for different periods (summation over *j*), the subscripts H_{ox} and H_{oy} refer to polarizations of the primary wave magnetic field. We used the Nelder–Mead method for an optimization of object characteristics. The required parameters of the object include: depth h_n of its top buried beneath the sediments, thickness d_n, resistivity ρ_n of the medium inside, its rectangular sizes and shifts of its center in the polygon along *OX* and *OY* axes.

To speed up the process, it was carried out in two steps. At the first stage the optimum center of starting heterogeneity was defined by cycle forward through all points of the large grid. The choice of the

object center location relative to the observation points was terminated when results of calculations with changed starting models matched. Further optimization of other parameters of an object was performed using the Nelder–Mead method. The result reliability was also estimated by its dependence on starting models. Thus, searching the crustal 3D-object was implemented.

For example, Fig. 4c the shows the optimum model of 3D-heterogeneity. The distribution of the TM-mode potential on the sea ice surface is given in Fig. 4d (the period of 139 s, the primary wave magnetic field polarization along the *OY* axis). In Figs 4e and f, the specified lines show the dependences of TM-mode potential on the period received in this case for sites 72 and 40 (let's notice that U^{TM}=0 in site 72 for the primary wave magnetic field polarization along the *OX* axis). The optimal object parameters are d_n=1.9 km, h_n=0.5 km and ρ_n=170 Ohm·m. They are close to input parameters, however do not completely coincide with them, because of the existing similar object models equivalence area. In particular, the obtained results depend on the number of sites and their positions in relation to the heterogeneity center. Changing these data allows obtaining other optimum parameters of an object. All of them will form the area of object model equivalences. In addition, we determined optimum parameters for the rough model of heterogeneity. Input data are calculated for the more complex heterogeneity structure. Therefore, we have misfits between model and experimental curves as shown in Figs 4e and f which do not depend on the starting model of the heterogeneity. The quality of restoration depends on the a priori information on the object and the available measurements. Restoring the object's properties affecting the measurement data is also possible. We propose to use additional methods to improve the result reliability.

ANALYTICAL CONTINUATION OF PROFILE DATA

The analytical continuation method can be applied to the acquisition of data on the object depth. In geophysics, continuation of gravitational and magnetic fields is applied to determining the source location in the lower half-space using the surface data. However, for near surface sources of gravitational and magnetic fields, here arises the instability of the algorithms based on the representation of fields in the form of Taylor decompositions, the Fourier series or integrals like Cauchy. For elimination of the arising difficulties, Ermokhin (2017) suggested a method based on the theory of continued fractions. To check its applicability to the MTS method we made numerical experiments with synthetic data for the considered conductivity model (using the profile data).

Let's briefly outline features used in (Ermokhin 2017) the algorithm. Results of measurements of a field parameter f_k on the profile are presented by a series of the Chebyshev polynomial of the first kind $T_n(x)$ on the interval of -1≤*x*≤1 (the transition to new coordinate *x* is carried out by scaling of coordinates of *k*-th points of the profile):

$$f(x) = \sum_n c_n T_n(x), \;\; T_n(x) = \cos(n \arccos x), \;\; -1 \le x \le 1 . \qquad (4)$$

The c_n coefficients were found by the least-square method. At the rare measurement net it is possible to apply the data interpolation by means of cubic splines. The series (4) will be transformed further to a continued fraction using the Viskovatov method (Baker & Graves-Morris 1996; Ermokhin 2017) and represented in the form:

$$F(x) = \cfrac{1}{1 + \cfrac{a_1 Y}{1 + \cfrac{a_2 Y}{1 + \cfrac{a_3 Y}{1 + \cdots}}}}, \;\; Y = \exp(i \arccos x), \qquad (5)$$

where the a_n coefficients are defined by the c_n set so that $f(x) \approx Re[F(x)]$ at the real *x* values (preliminary we normalized $f(x)$ so that $\max\{f(x)\}$=1). Further transition was carried out in (5) to the complex variable $x + iz$, where *z* is a depth. The received complex function $F(x,z)$ is an analytical continuation of $f(x)$, and isolines of the module $|F(x,z)|$ reflect the distribution of its singular points in the lower half-space. These points correspond to sources of the anomalous field in the medium. The described algorithm will be stable when calculating an analytical continuation owing to properties of continued fractions. The length of a continued fraction or the number of taken a_n is defined by stability of the results obtained on the *n* increase.

We carried out an analytical continuation of synthetic data for the model shown in Figs 4a and b. The used data on the potential of $U^{TM}(x,y)$ (the period of 139 s, the primary wave magnetic field polarization along the *OY* axis) on several profiles parallel to the *OX* axis are shown in Fig. 5a. Changes of the complex potential of the TM-mode along the given profile are presented in Fig. 5b. For an analytical continuation, the data on the real part of the potential are taken, since its imaginary part is much

less. To check this, the potential value modules were used. This change did not affect results of data analytical continuation in the described way. The length of the continued fraction was taken to be 95, since as at proximate values the discussed results did not change.

We calculated the modules $|F(x,z)|$ distributions on several profiles parallel to the *OX* axis using (5) (preliminary all functions $f(x)$ were normalized so that $\max\{f(x)\}=1$, therefore, all functions $F(x,z)$ are dimensionless). Further we interpolated these functions across profiles for several depths near maxima of $|F(x,z)|$. The distance between profiles is equal to 270 m (this value is step of the data interpolation by cubic splines in (4)).

The joint distribution of the anomalous field source depths in the model received according to data of several parallel profiles is shown in Fig. 5c. At display of distributions the return scaling on axes of coordinates was applied. It is established that for the coincidence of results of an analytical continuation to the true depth of the object upper surface (in the chosen medium model it is 1.7 km) it is necessary to enter, in addition, a correction multiplier reducing scalable depths at 5.25 time. For a clarification of the factors influencing the values of this multiplier, additional calculations for the medium model with the reduced sea depth up to 0.5 km and other parameters were unchanged. The resultant distribution is given in Fig. 5d. It is established that reduction in the sea depth does not exert any influence on the value of correction multiplier at the return scaling on the *OZ* axis. Also, calculations for the initial chosen medium model with reduced (up to 91) quantity of reference points along *OX* and *OY* axes were carried out. The results obtained in this case coincide with the results shown in Fig. 5. Besides, the calculations with the change of the 3D-heterogeneity model (Fig. 6) are carried also out. Again, the calculated data are taken about the potential of $U^{TM}(x,y)$ (the period of 139 s, the primary wave magnetic field polarization along the *OY* axis) on the profiles parallel to the *OX* axis (Figs 6a and b). The 3D-heterogeneity model is taken with the plan projection (Fig. 6c). The length of the continued fraction equals 60 is chosen from the stability of analytical continuations. The joint distribution of the anomalous field source depths in this model received according to data of several parallel profiles is shown in Fig. 6d. It also reflects the depths of sources along the *OY* axis. The change of the 3D-heterogeneity model did not affect the value of the correction multiplier at the return scaling on the *OZ* axis. The depths of the anomalous field sources coincide with the crustal 3D-object positions in these models with the application of the same correction multiplier of 5.25.

We found the value of a correction multiplier depends on the choice of the polygon sizes. It is clear because these sizes determine the profile lengths and the data set with measurement results for analytical continuation. For real data, we can check the correction multiplier of the return scaling on the *OZ* axis using simulation conditions close to experimental.

Thus, the application of the analytical continuation method helps to localize of the crustal 3D-heterogeneity.

THE CED APPLICATION FOR MEASUREMENTS ON THE ICE SURFACE ON THE OB RIVER

We carried out preliminary measurements on the ice surface on the Ob river in March, 2019 to check out possibilities of the MTU-5 Phoenix Geophysics standard station for the CED system application. In this case, we definitely did not take into account the ice drift. In addition, at our latitude there are no non-plane-wave effects. It was only the first experiment.

The holes were drilled in the ice for placement of electrodes, to get a good coupling to the water. We used non-polarizable electrodes. Resistance of ground electrodes in water was small. Signal value on long lines (up to 500 m and more) was increased. Operating conditions of the MTU-5 station differed from typical. We established that it is possible to provide the normal operating conditions of the MTU-5 station, including additional resistance of 1 kΩ in the CED radial lines.

For the comparison of the digital and analog compensation of signals of the CED lines we made experiments, using two different schemes. In one option we connected to electric channel of the MTU-5 station the CED full system consisting of eight radial lines (Fig. 1) with additional resistances. In other option we used two MTU-5 stations. We connected separately four lines of the North-South and West-East directions from the CED to four electric channels of two stations. This option provided for application of digital compensation of four lines signals. We established that the amplitude of the analog signal compensation at 8-10 times surpasses results of the digital signal compensation.

We carried out an inspection of the measurement results of the TM-mode potential by the CED. For this purpose, we used the MTS data obtained earlier near the CED system (54°38´ N, 82°42´ E). Positions of two MTS points relative to the CED center are shown in Fig. 7a. We solved an inversion problem to define a geoelectric model near the CED system. For this purpose, we applied also the algorithm of the forward problem solution using the Trefftz method (Plotkin & Gubin 2015). We carried

out the inversion of the apparent resistivity curves in two MTS points by minimizing the functional Φ which defines residuals between the calculated and measured curves:

$$\Phi = \frac{1}{2KJ}\sum_{k=1}^{K}\sum_{j=1}^{J}\left(\left|\frac{lg\rho_{xy}^{t} - lg\rho_{xy}^{0}}{lg\rho_{xy}^{0}}\right|^{2} + \left|\frac{lg\rho_{yx}^{t} - lg\rho_{yx}^{0}}{lg\rho_{yx}^{0}}\right|^{2}\right)_{k,j},$$

where $\rho_{xy}^{t}, \rho_{xy}^{0}, \rho_{yx}^{t}, \rho_{yx}^{0}$ are the apparent resistivities (the subscripts *xy* and *yx* denote different field polarizations, and superscripts t and 0, refer to the simulated and experimental apparent resistivities respectively), obtained at different stations (summation over *k*) and for different periods (summation over *j*), We used the Nelder–Mead method for an optimization. The experimental and model curves of the apparent resistivity are shown in Figs 7e and f (residuals are specified for each point).

The found 3D-medium model is presented in Figs 7b, c and d. The Cartesian coordinate system with the origin in the CED position was used (the *OX* axis is directed to the north, the *OY* axis – to the east, the *OZ* axis - vertically with positive down, the ice surface of z = 0). We used the one-dimensional starting model received by an inversion of the ρ_{xy} curve in p.06 (Fig. 7f). It is the three-layer medium model with electric resistivities of 161, 2301 and 484 Ohm·m and layer thicknesses of 0.21, 2.24 and 24.74 km (from top to down). The resistivity of the underlying layer is equal to 32,594 Ohm·m. During the 3D-model optimization, we varied the layer thicknesses, the resistivity of the underlying layer and lateral distributions of the resistivity in layers. Using the Trefftz method each layer is represented by 25 identical parallelepipeds having uniform conductivities, and their heights are equal to the layer thicknesses. Horizontal sections of parallelepipeds are 8x8 km. The number of parallelepipeds placed along each horizontal axis is 5. The polygon sizes are 40x40 km. We changed resistivity in each parallelepiped. The total number of the varied parameters is equal to 79=3+1+3x25.

In the found 3D-medium model, the layer thicknesses are equal to 0.11, 2.08 and 3.35 km (from top to down). The resistivity of the underlying layer is equal to 100,000 Ohm·m. Note that for regularization of the inversion problem we limited an interval of resistivity values with a range from 1 to 100,000 Ohm·m.

Further we compare the TM-mode potential calculated for the found 3D-medium model to the CED experimental data. We carried out the U^{TM} potential calculation using (1)-(2). The TM-mode potential excited in 3D-medium depends on polarization of vertically propagating primary wave. For accounting this circumstance, we entered the ratio similar to impedance:

$$U^{TM} = K_x E_x + K_y E_y.$$

For the found 3D-medium model, we calculated coefficients $K_{x,y}(\omega, x, y)$ using the primary wave polarizations respectively. Fig. 7g shows the found dependences of $K_{x,y}$ on the period for the CED center. Further we calculated the U^{TM} potential for recorded polarizations of the primary wave, using data of the component $E_{x,y}(\omega)$ measurements. The calculated and measured U^{TM} potential dependences on the period are presented in Fig. 7h. Obviosly, there is a compliance between the dependences on the period measured by the CED with 4 both 8 lines and calculated for the found 3D-medium model. It should be noted such coincidence of curve dependences on the period was achieved after their shift on ordinate axis. For this purpose, we used the coefficients considering distinction of the signal values registered by the various CED installations.

CONCLUSIONS

We believe the recording of the additional data on the electric field TM-mode potential at magnetotelluric sounding in the Arctic allows to define both the existence and characteristics of crustal conductivity 3D-heterogeneities. These objects cannot almost be found at standard magnetotelluric sounding owing to their shielding by conductive layers of seawater and sediments. The related changes of the apparent resistivity are only one-hundredths of percent. The vertical magnetic field amplitudes caused by such crustal objects are very small. We showed that the electric field potential of the TM-mode reaches values suitable for detection. Using such data obtained in several points allows to solve the inverse problem and to determine the properties of the crustal 3D-object.

The additional data on the 3D-object depth can be obtained also by the analytical continuation of the profile data on the TM-mode electric field potential. We proved this concept by numerical

experiments with synthetic data using the analytical continuation method based on the theory of continued fractions.

Recording the CED data by the MTU-5 Phoenix Geophysics standard stations, we carried out preliminary measurements on the ice surface on the Ob river. By checking the measurement results of the TM-mode potential we revealed a compliance between the dependences measured by the CED and calculated for the 3D-medium model found according to the MTS data.

During our synthetic experiments, the measurement were made in a static location. Further we assume to consider the CED system movements by the drifting ice floes. To take into account the effect of these horizontal movements, we hope to accompany all recorded time series with coordinates of measurement points and to develop a technique for such data processing. By doing so we hope that the non-plane-wave effects will be taken into consideration as well.

ACKNOWLEDGEMENTS

The study was financially supported by the Russian Science Foundation (RSF), project no. 18-17-00095. We are grateful to Ute Weckmann and two anonymous reviewers for detailed comments and constructive reviews, which have substantially improved our manuscript.

FIGURE CAPTIONS:

Figure 1. Ideal (left) and real (right) circular electric dipole on the Earth's surface.

Figure 2. Deep section (a) and example of heterogeneity plan that is object target under ocean floor (b). Points in which fields are defined are shown. Designations are belonging: ρ_1, d_1 to seawater, ρ_2, d_2 to sediment, ρ_3, d_3 to crust, ρ_4 to mantle and ρ_n, d_n, h_n to object.

Figure 3. Dependences of modules of the TM-mode potential, apparent resistivity and vertical magnetic field component on period (left) in points specified by cross on distribution maps of these values for period of T=139 s (right). Medium model is shown in Fig. 2, 3D-object parameters are ρ_n =1000 Ohm·m, d_n=2.8 km, h_n=0.2 km. Polarization of primary wave magnetic field is along *OY* axis, its amplitude is 1 nT.

Figure 4. 3D-heterogeneity plan (a) and synthetic data calculated for it on small grid (b, e and f). Results of optimization received on the large grid (c, d, e and f). Optimal 3D-heterogeneity model (c) and dependences on period of the TM-mode potential in sites 72 and 40 (e and f) (misfits are specified for polarizations of primary wave magnetic field along *OY* and *OX* axes). Distributions of TM-mode potential at *z*=0 for period of *T*=139 s (b and d).

Figure 5. Map of $|U^{TM}(x,y)|$ for period of *T*=139 s (a) with profile shown in white color from which are taken data (b) for their analytical continuation $|F(x,z)|$, reflecting depth of anomalous field source in the medium, joint distribution of such depths according to data of several parallel profiles (c), dotted line shows the actual 3D-object roof. The map of isolines (d) similar (c) constructed by the results received for background model of the medium with the reduced sea depth of 0.5 km. Polarization of magnetic field of primary wave along *OY* axis.

Figure 6. Map of $|U^{TM}(x,y)|$ for period of *T*=139 s (a) with profile shown in white color from which are taken data (b) for their analytical continuation $|F(x,z)|$, reflecting depth of anomalous field source in the model with the 3D-heterogeneity plan (c), joint distribution of such depths according to data of several parallel profiles (d), dotted line shows the actual 3D-object roof. Polarization of magnetic field of primary wave along *OY* axis.

Figure 7. The map of the experiment area (a), the three-layer medium model according to MTS which are carried out here earlier: lateral distributions of resistivities ρ_1, ρ_2 and ρ_3 in layers from top to down (b, c and d, depths of layer roofs are specified, resistivity of the underlying layer is equal to 100,000 Ohm·m, depth of its roof of 5.54 km), experimental and model curves of the apparent resistivity in the MTS points (e and f), dependences on the period of the calculated coefficients of the potential U^{TM} relation with horizontal components of the primary wave electric field (g) and the experimental and model dependences of the potential $|U^{TM}|$ on the period.

REFERENCES

Baker, G.A., Jr. & Graves-Morris, P.R., 1996. Padé Approximants, Cambridge University Press, Cambridge.

Beka, T.I., Smirnov, M., Bergh, S.G. & Birkelund, Y., 2015. The first magnetotelluric image of the lithospheric-scale geological architecture in central Svalbard, Arctic Norway, *Polar Research,* **34**, 26766.

Ermokhin, K.M., 2017. Analytical continuation of gravitational and magnetic fields through masses, *Doklady Earth Sciences,* **476**(1), 1054-1057.

Evans, S., Jones, A.G., Spratt, J. & Katsube, J. 2005. Central Baffin electromagnetic experiment (CBEX): Mapping the North American Central Plains (NACP) conductivity anomaly in the Canadian arctic, *Physics of the Earth and Planetary Interiors*, **150**(1-3),107-122.

Fütterer, D.K., 1992. ARCTIC'91: The Expedition ARK-VIII/3 of RV "Polarstern" in 1991, *Reports on Polar Research,* **107**, 267 pp.

Goldman, M., Mogilatov, V., Haroon, A., Levi, E. & Tezkan, B., 2015. Signal detectability of marine electromagnetic methods in the exploration of resistive targets, *Geophysical Prospecting*, **63**(1), 192-210.

Hill,G.J., 2018. EM Studies in Polar Regions, *Abstract, 24th EM Induction Workshop*, *Helsingør, Denmark, August 12-19, 2018.*

Hoffman, A.A.J. & Horton, C.W., 1966. An analysis of some magnetotelluric records from Tikhaya Bay, U.S.S.R., *Journal of Geophysical Research,* **71**(16), 4047-4052.

Korotaev, S.M., Zhdanov, M.S., Orekhova, D.A., Kruglyakov, M.S., Trofimov, I.L., Schors, Yu.G. & Shneyer, V.S., 2010. Study of the possibility of the use of the magnetotelluric sounding method in the Arctic Ocean with quantitative modeling, *Izvestiya, Physics of the Solid Earth*, **46(**9), 759–771.

Mogilatov, V., Goldman, M., Persova, M., Soloveichik, Yu., Koshkina, Yu., Trubacheva, O. & Zlobinskiy, A., 2016. Application of the marine circular electric dipole method in high latitude Arctic regions using drifting ice floes, *Journal of Applied Geophysics,* **135**(S1), 17–31.

Piskunova, E.A., Palshin, N.A. & Yakovlev, D. V., 2018. Electrical conductivity features of the Arctic shelf permafrost and electromagnetic technologies for their studies, *Russian Journal of Earth Sciences*, **18**(5), ES5001,1-14.

Plotkin, V.V., 2017. Fast computation of MT curves for a horizontally layered earth with laterally inhomogeneous conductivity perturbations, *Russian Geology and Geophysics*, **58**(11), 1441-1451.

Plotkin, V.V., Belinskaya, A.Y. & Gavrysh, P.A., 2011. Nonlocal electromagnetic response: Implications in the regional sounding, *Izvestiya. Physics of the Solid Earth*, № 1, 23-32.

Plotkin, V.V. & Gubin, D.I., 2015. Accounting for near-surface inhomogeneities over a horizontally layered section in magnetotelluric sounding, *Russian Geology and Geophysics*, **56**(7), 1083-1090.

Plotkin, V.V. & Mogilatov, V.S., 2019. About Registration of Vertical Component of Electric Field at Magnetotelluric Sounding, *Russian Geology and Geophysics* **60**(12), (in press).

Plotkin, V.V. & Mogilatov, V.S., 2020. About Measurement of Vertical Component of Electric Field During Magnetotelluric Sounding, *in: Yanovskaya T., Kosterov A., Bobrov N., Divin A., Saraev A., Zolotova N. (eds), Problems of Geocosmos-2018. Springer Proceedings in Earth and Environmental Sciences*, Springer, Cham, ISBN 978-3-030-21788-4, https://doi.org/10.1007/978-3-030-21788-4_4, 29-37, https://link.springer.com/chapter/10.1007%2F978-3-030-21788-4_4

Swift, D.W. & Hessler V.P., 1964. A comparison of telluric current and magnetic field observations in the Arctic Ocean., *Journal of Geophysical Research*, **69**(9), 1883-1893.

Thiede, J., 2002. POLARSTERN ARKTIS XVII/2 Cruise Report: AMORE 2001 (Arctic Mid-Ocean Ridge Expedition), *Reports on Polar and Marine Research*, **421**, 397 pp.

Trofimov, I.L. & Fonarev, G.A., 1976. Deep magnetotelluric surveys in the Arctic ocean. *Geoelectric and Geothermal Studies*, Akadémiai Kiadó, Budapest.

Wannamaker, P.E., Stodt, J.A. & Olsen, S.L., 1996. Dormant state of rifting below the Byrd Subglacial Basin, West Antarctica, implied by magnetotelluric (MT) profiling, *Geophysical Research Letters*, **23,** 2983–2986.

Wannamaker, P.E., Stodt, J.A., Pellerin L., Olsen, S.L. & Hall D.B. 2004. Structure and thermal regime beneath the South Pole region, East Antarctica, from magnetotelluric measurements, *Geophys. J.Int.*, **157, 3**6–54.

Wannamaker, P., Hill, G., Stodt, J., Maris, V. Ogawa, Y., Selway, K., Boren, G., Bertrand, E., Uhlmann, D., Ayling, B., 2017. Uplift of the central transantarctic mountains, *Nature Communications,* **8,** 1588, DOI: 10.1038/s41467-017-01577-2.

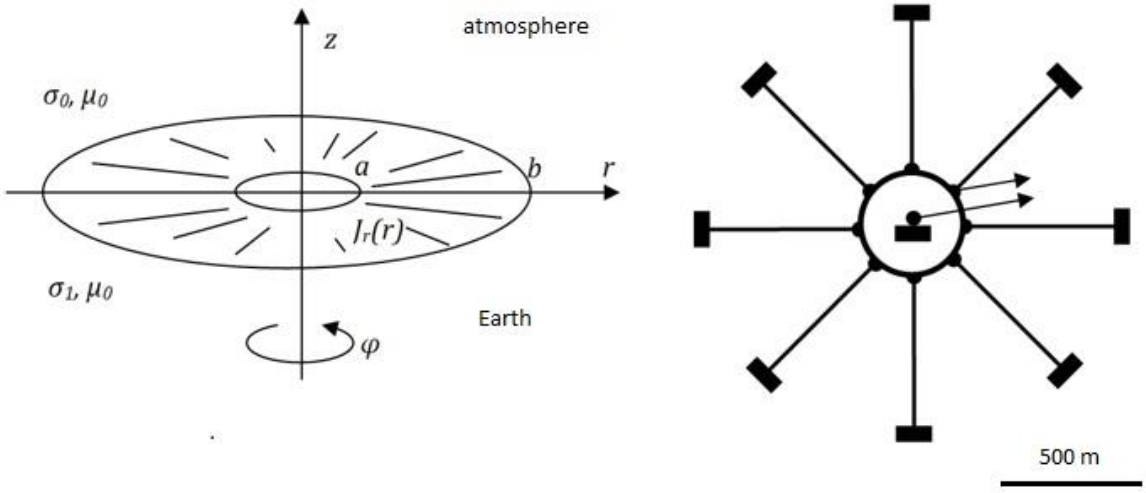

Figure 1. Ideal (left) and real (right) circular electric dipole on the Earth's surface.

a

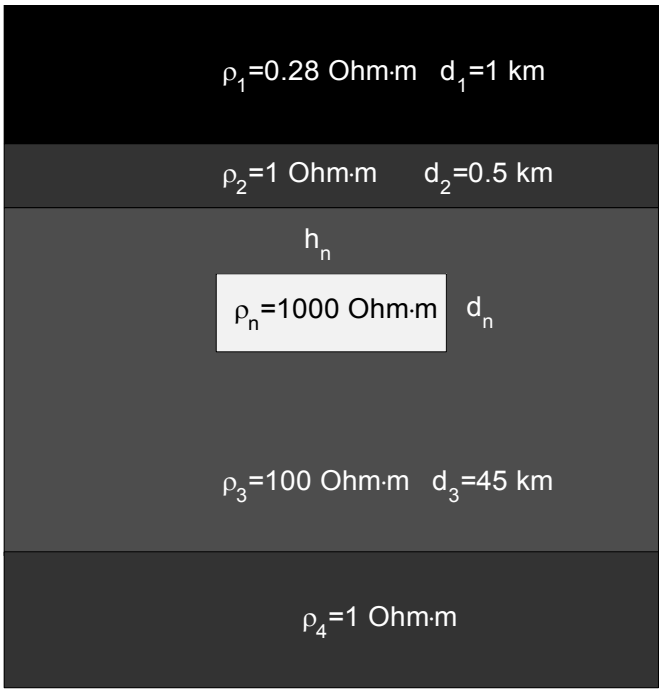

b

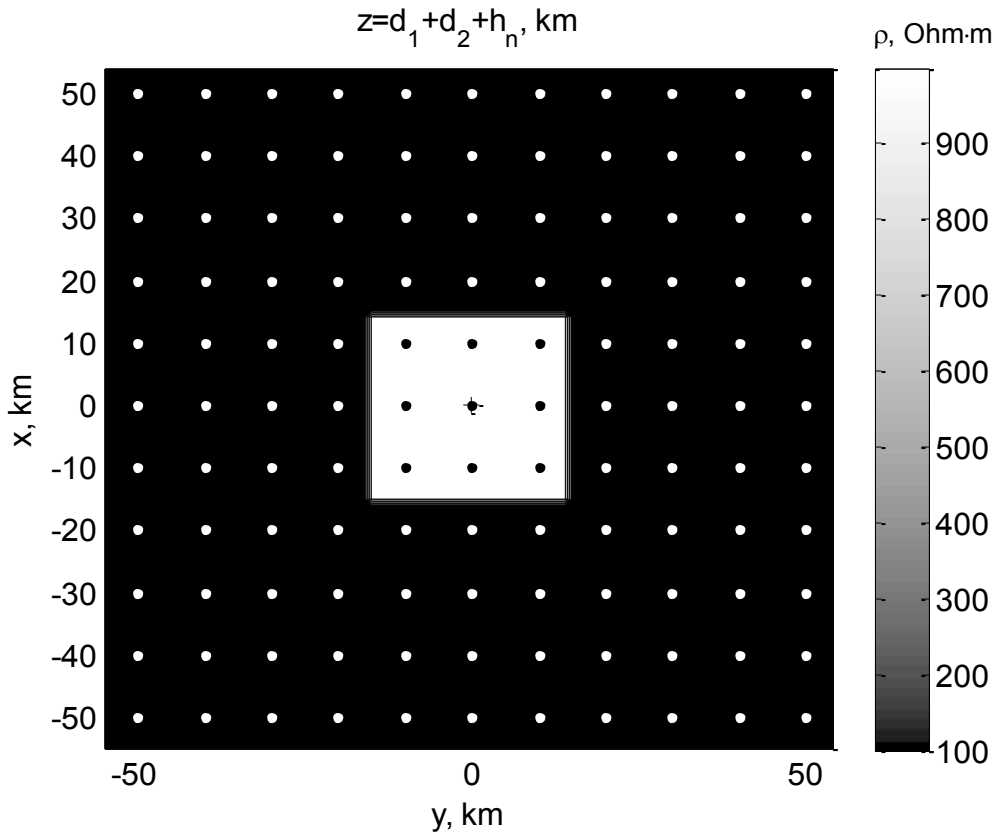

Figure 2. Deep section (a) and example of heterogeneity plan that is object target under ocean floor (b). Points in which fields are defined are shown. Designations are belonging: ρ_1, d_1 to seawater, ρ_2, d_2 to sediment, ρ_3, d_3 to crust, ρ_4 to mantle and ρ_n, d_n, h_n to object.

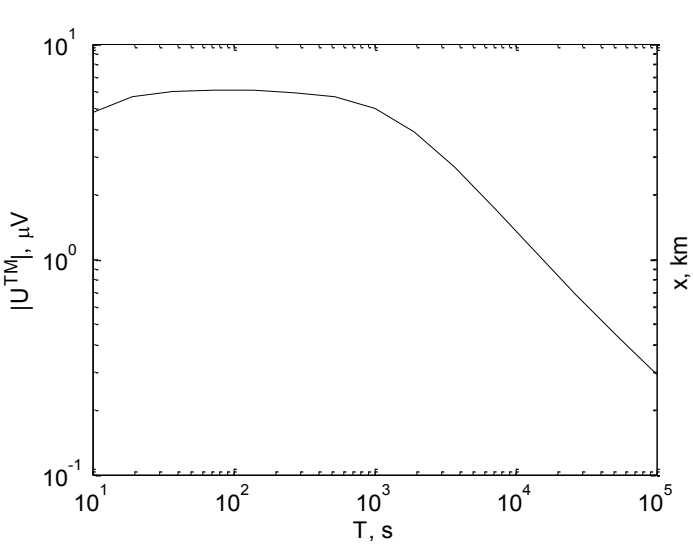

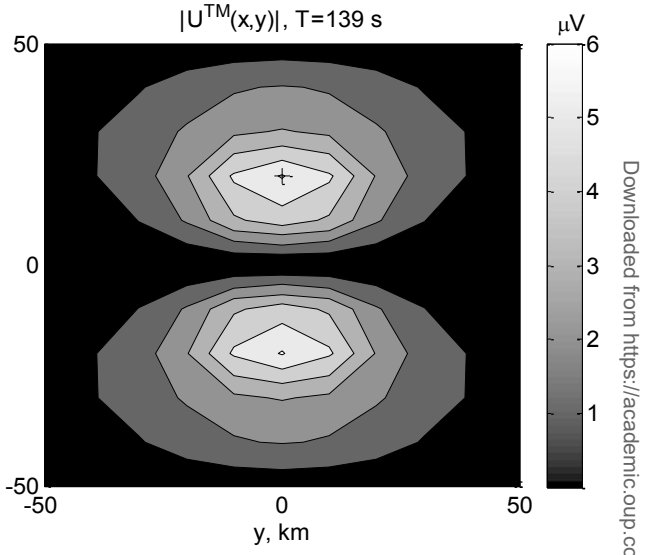

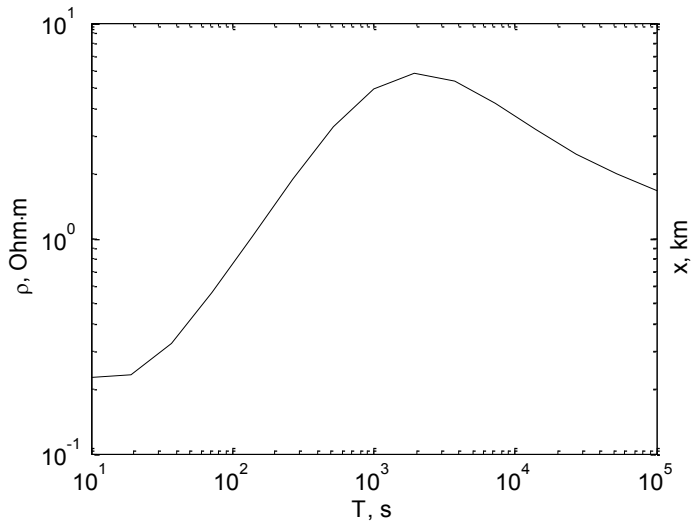

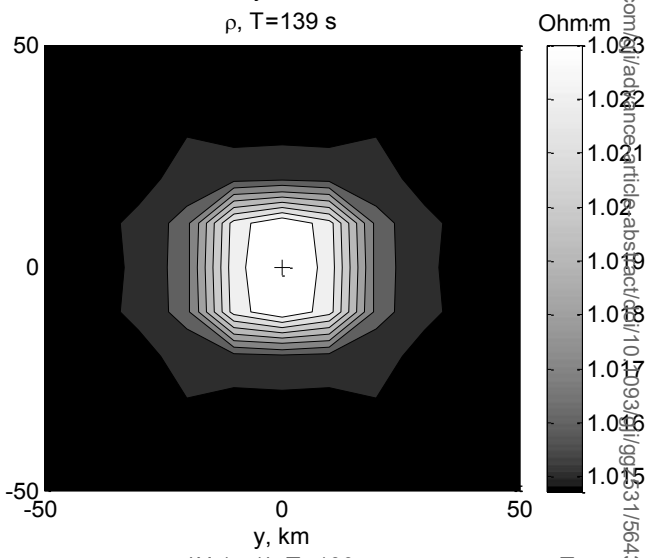

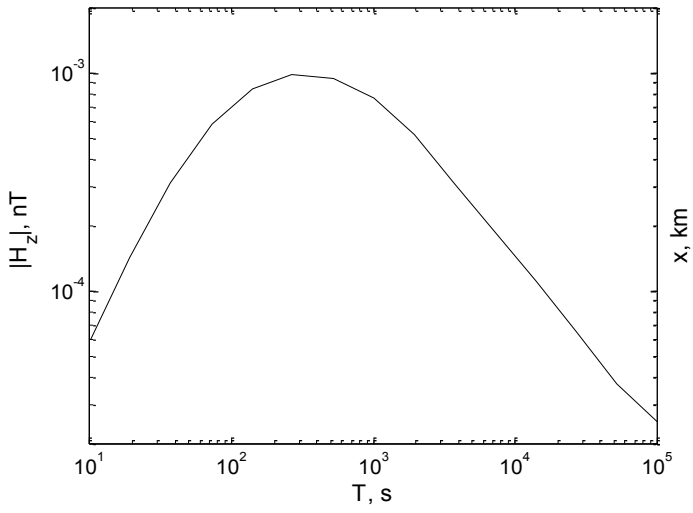

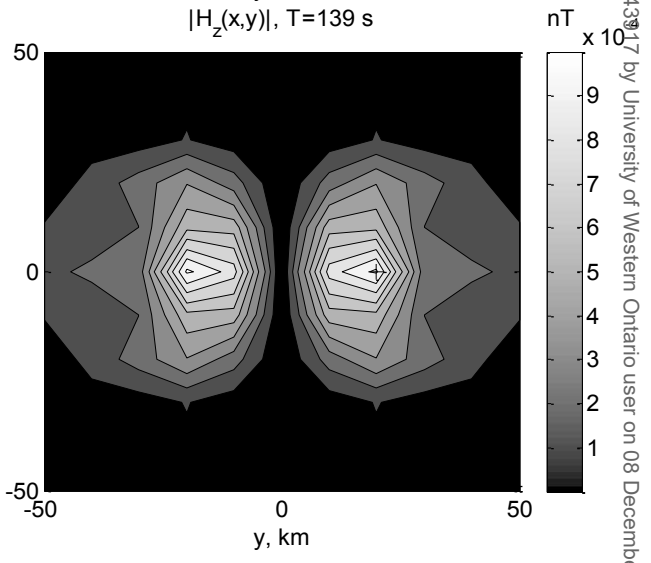

Figure 3. Dependences of modules of the TM-mode potential, apparent resistivity and vertical magnetic field component on period (left) in points specified by cross on distribution maps of these values for period of T=139 s (right). Medium model is shown in Fig. 2, 3D-object parameters are ρ_n =1000 Ohm·m, d_n=2.8 km, h_n=0.2 km. Polarization of primary wave magnetic field is along *OY* axis, its amplitude is 1 nT.

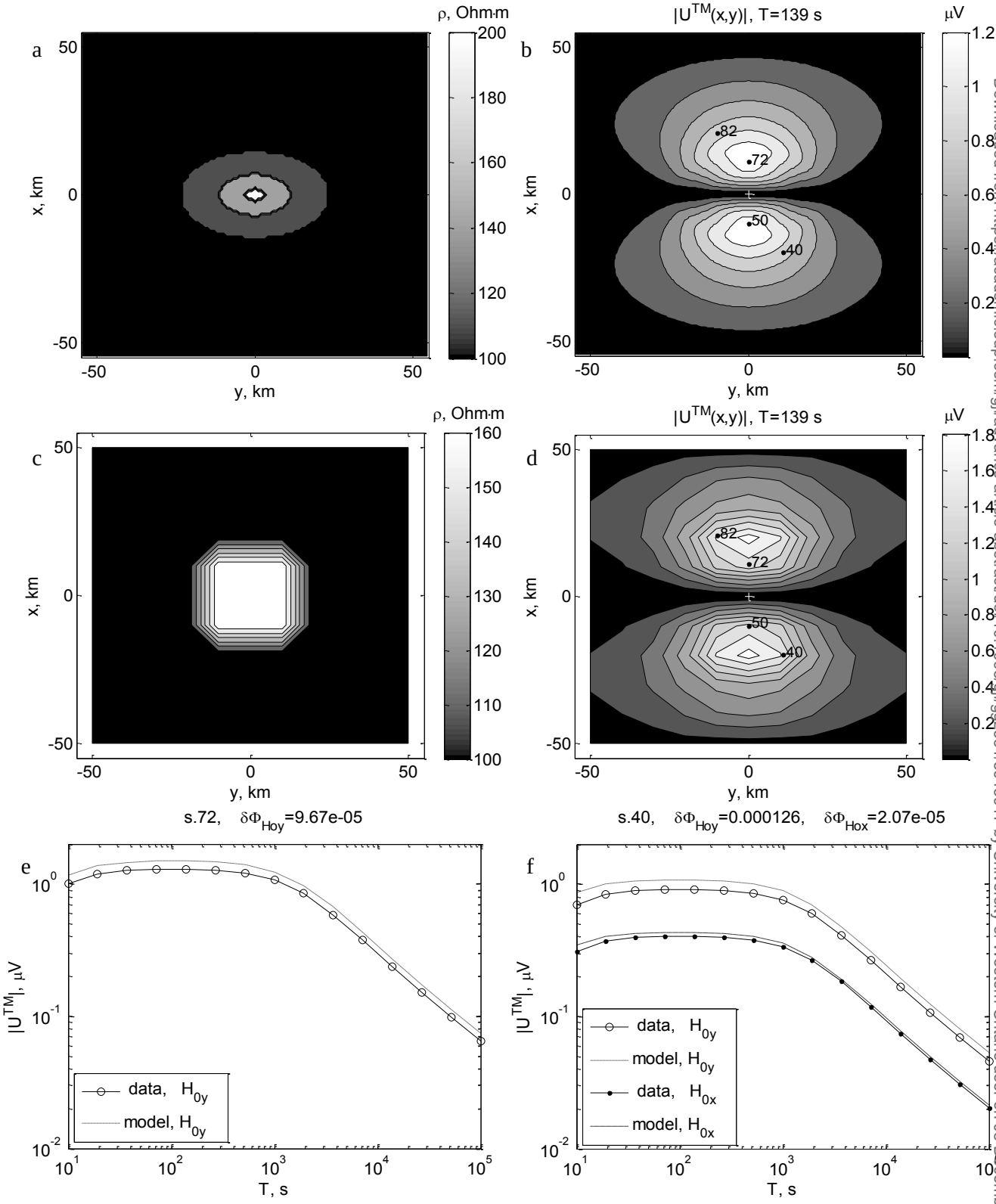

Figure 4. 3D-heterogeneity plan (a) and synthetic data calculated for it on small grid (b, e and f). Results of optimization received on the large grid (c, d, e and f). Optimal 3D-heterogeneity model (c) and dependences on period of the TM-mode potential in sites 72 and 40 (e and f) (misfits are specified for polarizations of primary wave magnetic field along *OY* and *OX* axes). Distributions of TM-mode potential at z=0 for period of T=139 s (b and d).

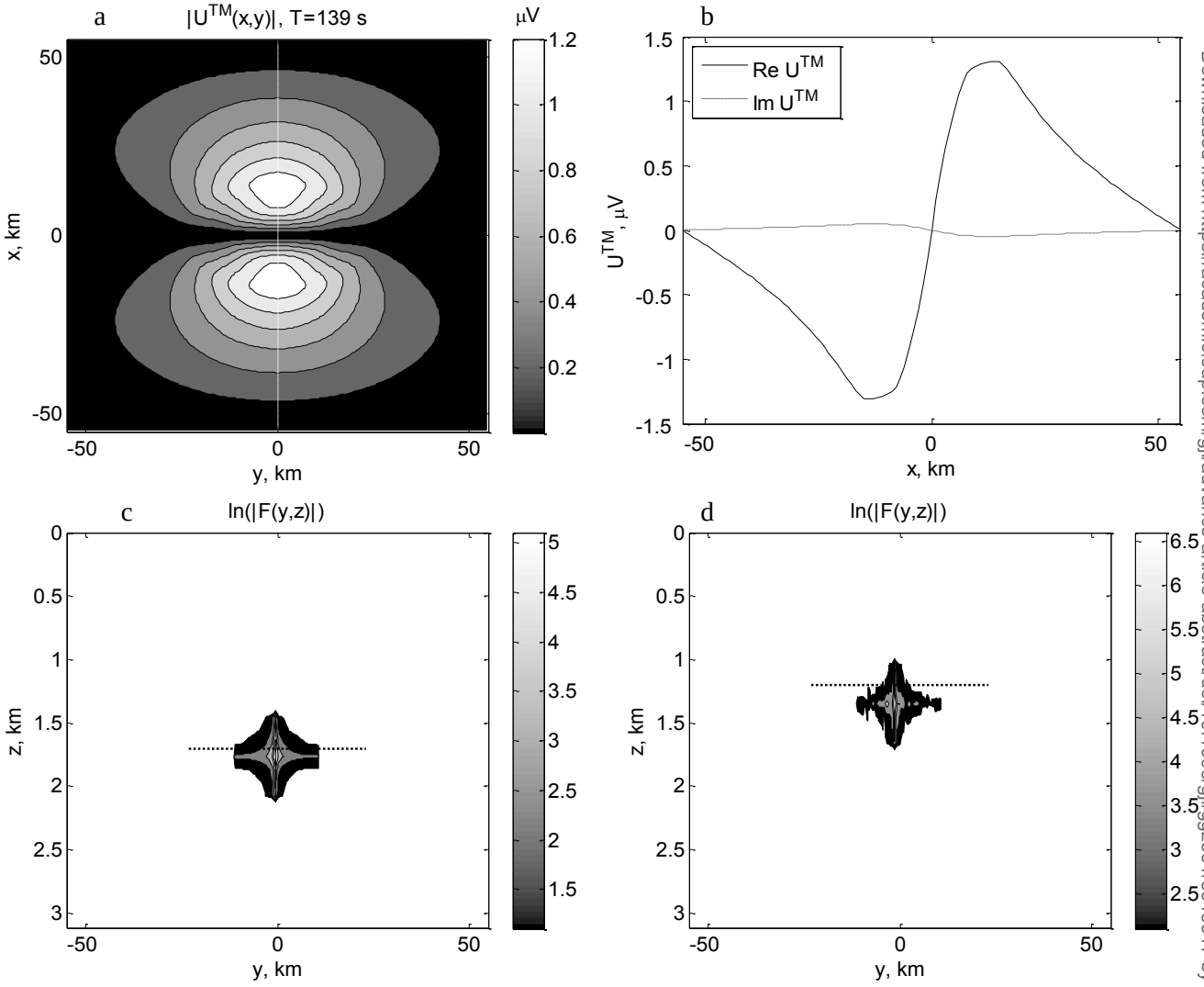

Figure 5. Map of $|U^{TM}(x,y)|$ for period of *T*=139 s (a) with profile shown in white color from which are taken data (b) for their analytical continuation $|F(x,z)|$, reflecting depth of anomalous field source in the medium, joint distribution of such depths according to data of several parallel profiles (c), dotted line shows the actual 3D-object roof. The map of isolines (d) similar (c) constructed by the results received for background model of the medium with the reduced sea depth of 0.5 km. Polarization of magnetic field of primary wave along *OY* axis.

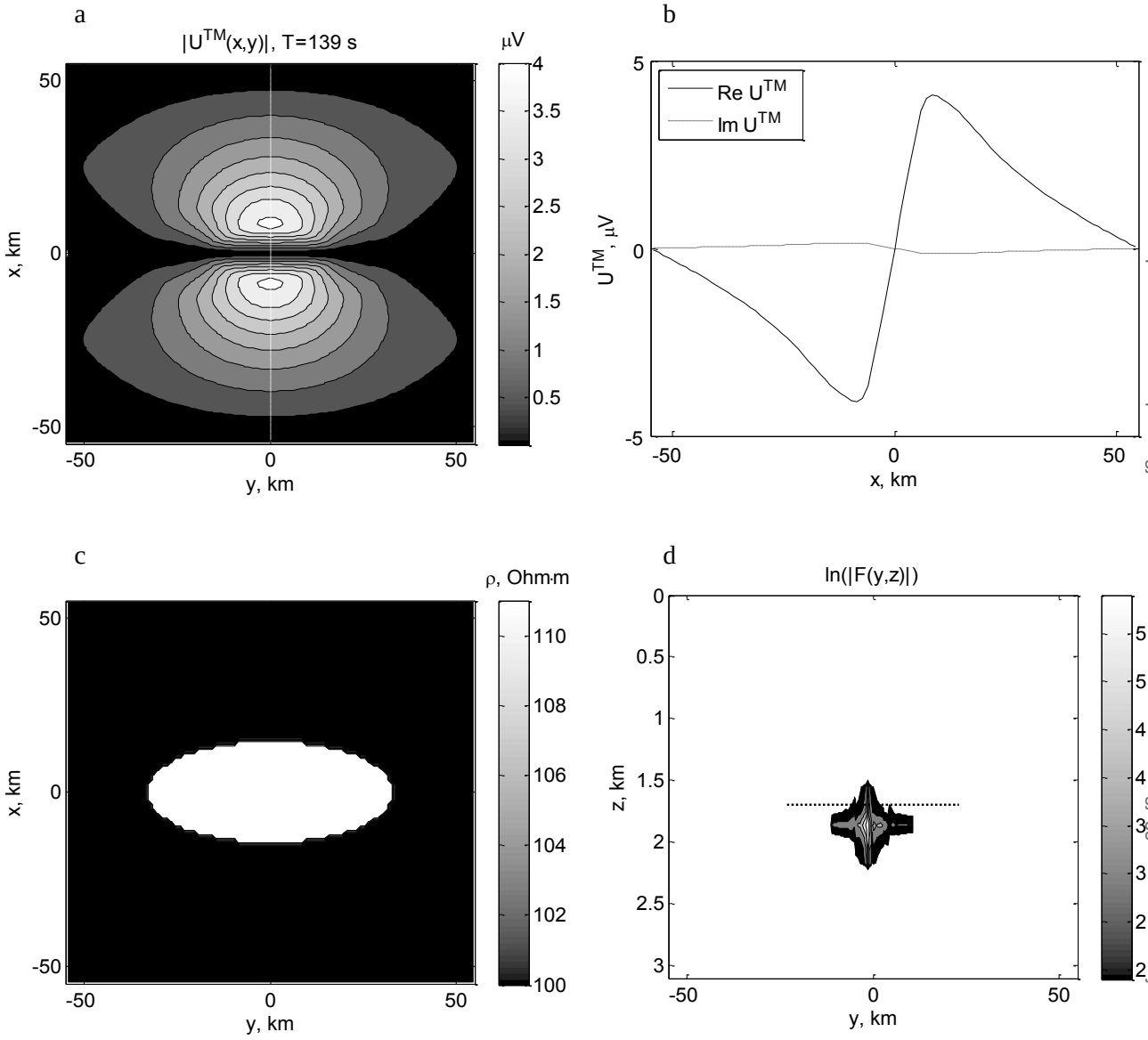

Figure 6. Map of $|U^{TM}(x,y)|$ for period of *T*=139 s (a) with profile shown in white color from which are taken data (b) for their analytical continuation $|F(x,z)|$, reflecting depth of anomalous field source in the model with the 3D-heterogeneity plan (c), joint distribution of such depths according to data of several parallel profiles (d), dotted line shows the actual 3D-object roof. Polarization of magnetic field of primary wave along *OY* axis.

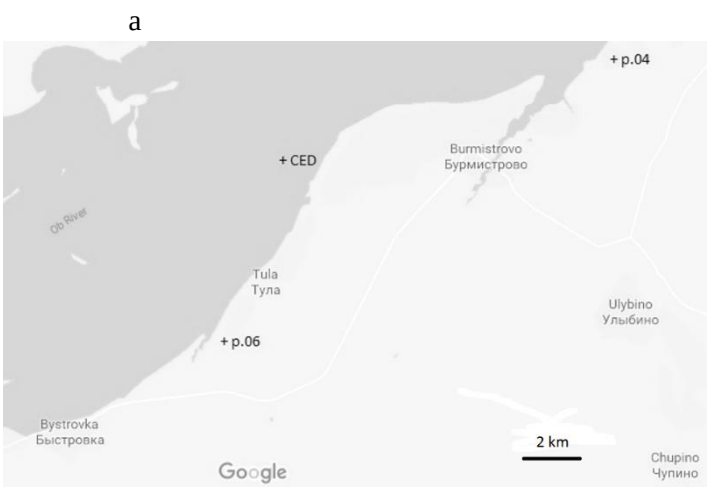

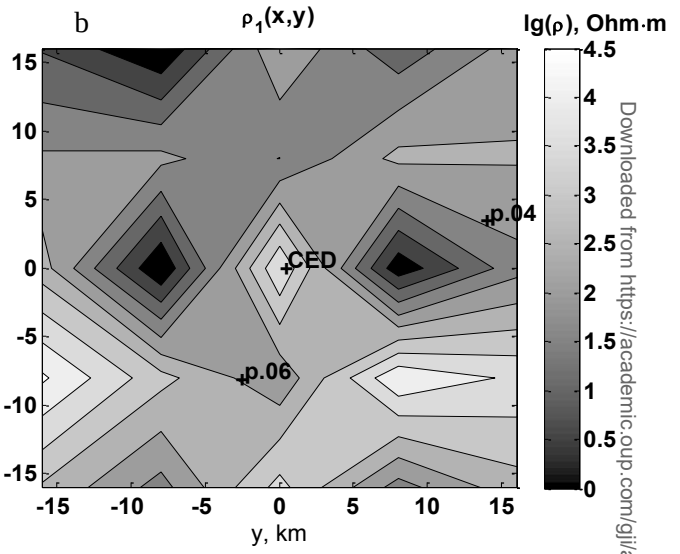

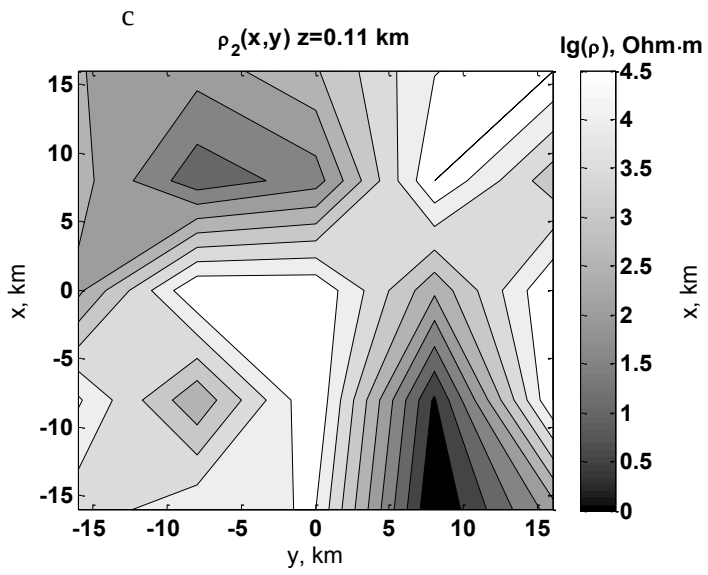

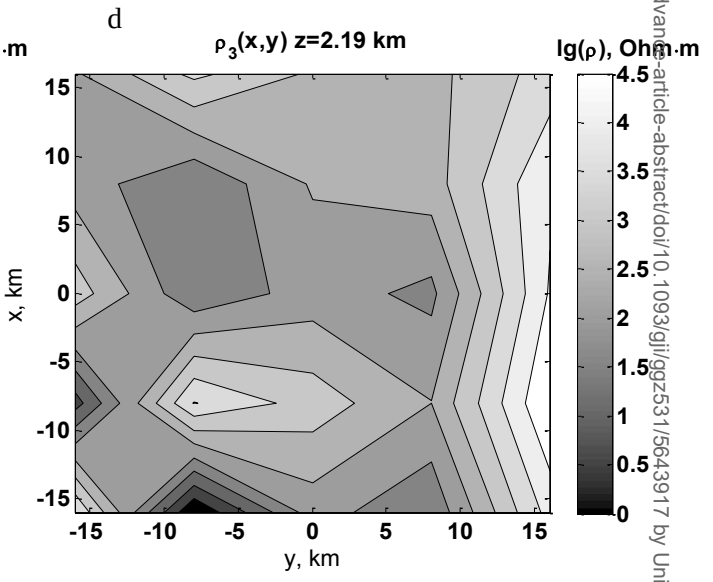

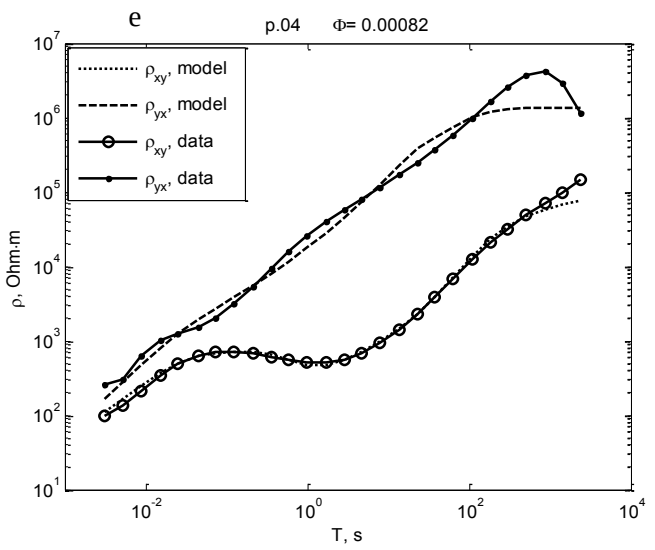

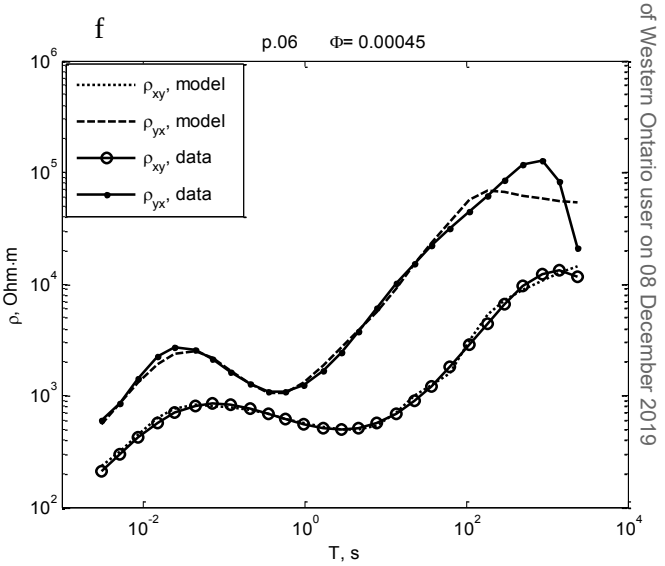

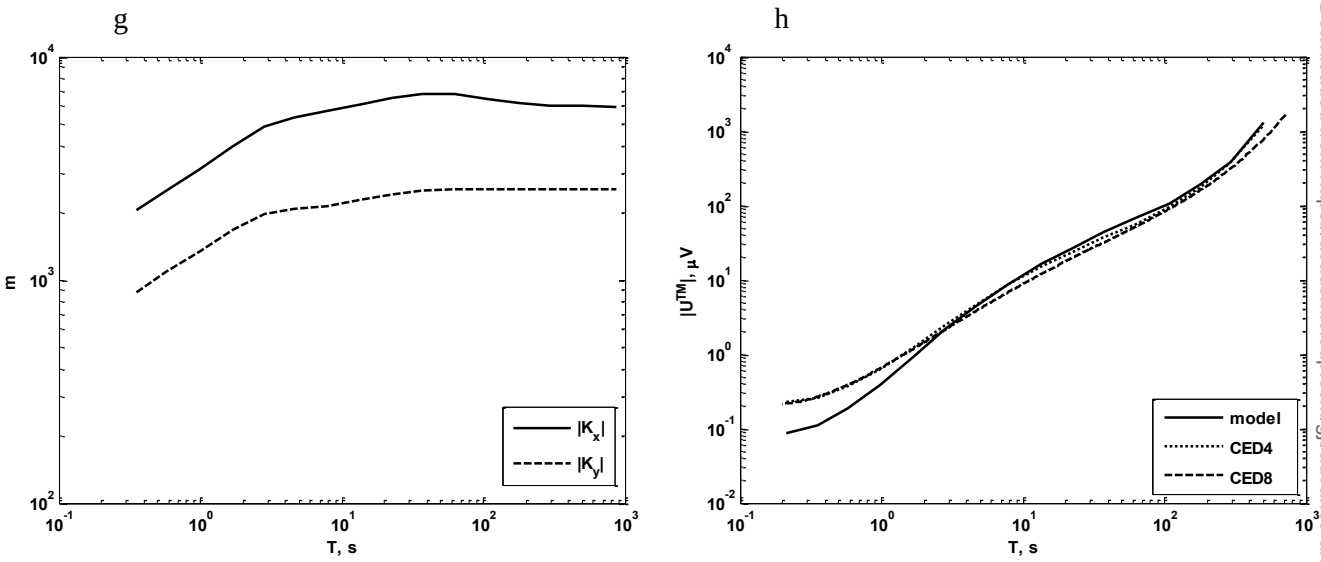

Figure 7. The map of the experiment area (a), the three-layer medium model according to MTS which are carried out here earlier: lateral distributions of resistivities ρ_1, ρ_2 and ρ_3 in layers from top to down (b, c and d, depths of layer roofs are specified, resistivity of the underlying layer is equal to 100,000 Ohm·m, depth of its roof of 5.54 km), experimental and model curves of the apparent resistivity in the MTS points (e and f), dependences on the period of the calculated coefficients of the potential U^{TM} relation with horizontal components of the primary wave electric field (g) and the experimental and model dependences of the potential $|U^{TM}|$ on the period.